Global and Planetary Change 107 (2013) 70–81

Contents lists available at SciVerse ScienceDirect

Global and Planetary Change

journal homepage: www.elsevier.com/locate/gloplacha

Interannual sea level variability in the tropical Pacific Ocean from 1993 to 2006

Qing Lu [a,b,*], Juncheng Zuo [a,b], Yanfang Li [c], Meixiang Chen [a,b]

[a] Key Laboratory of Coastal Disaster and Defence, Ministry of Education, Hohai University, Nanjing, Jiangsu, China
[b] Institute of Physical Oceanography, Hohai University, Nanjing, Jiangsu, China
[c] Yantai Institute of Coastal Zone Research, Chinese Academy of Sciences, Yantai, Shandong, China

ARTICLE INFO

Article history:
Received 21 December 2012
Accepted 21 April 2013
Available online 26 April 2013

Keywords:
Sea surface height
Tropical Pacific
Surface heating
Ekman pumping
Rossby waves

ABSTRACT

Three net surface heat flux products, namely from 1) version 2 of Common Ocean Reference Experiment (CORE.2), 2) Objectively Analyzed Air–Sea Fluxes (OAFlux), and 3) the European Centre for Medium-Range Weather Forecasts operational ocean analysis/reanalysis system (ECMWF ORA-S3), and three wind stress products, namely from 1) CORE.2, 2) Simple Ocean Data Assimilation Reanalysis, version 2.1.6 (SODA 2.1.6), and 3) ECMWF ORA-S3 are used to investigate the abilities of four simple oceanic mechanisms in explaining the interannual variance of altimetry-derived sea surface height (SSH) anomalies in the tropical Pacific Ocean over the period 1993–2006. It is found that local response to surface heating plays an important role in sea level rise along the western equatorial Pacific (150°–180°E). The dominant processes affecting interannual variability of observed SSH anomalies vary regionally in the tropical Pacific; local response to surface heating, local Ekman pumping, wind-induced first baroclinic mode Rossby waves and the eastern boundary forcing are all important. Both the local response to surface heating and the eastern boundary forcing are important in explaining the interannual variance of observed SSH anomalies in the northeastern tropical Pacific; while the dominant contribution to interannual sea level variability in the southeastern tropical Pacific is from the eastern boundary forcing, the local Ekman pumping plays a relatively minor role in the interannual SSH change there. The wind-induced first baroclinic mode Rossby waves dominate interannual SSH variability in the western tropical Pacific, excluding the area of 2°–10°N, west of 170°E. Although a large part of the interannual sea level variability in the western tropical Pacific is related to the oceanic remote adjustment to wind stress forcing, the contributions of local responses to surface heating and wind forcing cannot be overlooked.

1. Introduction

Sea level changes, especially the regional sea level changes have been the focus of many recent investigations. The tropical Pacific Ocean is a hotspot for most investigations. This is not only for its rapid rise which is 3 times larger than the mean value of the global sea level rise, in the western tropical Pacific over the past two decades, which has been a threat to the low-lying islands and coastlines, but also because even the subtle sea surface temperature (SST) changes in the western tropical Pacific Ocean may lead to significant variations in the vigor of the monsoon and the weather patterns across the Indo-Pacific basin (McBride et al., 2003). Sea level can serve as an important proxy of variations in ocean circulation and climate. So it is very necessary to understand the causes underlying the sea level variability. The causes of sea level variability are associated with dynamic variations in the oceanic circulations caused by climate variability and with an isostatic adjustment of the Earth's crust. In addition, the effects of some processes such as anthropogenically-induced subsidence and earthquakes can't be neglected on the coastal regions (Stammer et al., 2013).

Numerous studies with data analysis, numerical modeling, and data assimilation have been devoted to determine the contributions of the different forcings to sea surface height (SSH) variability. The dominant processes affecting SSH variability vary with period and latitude. Vivier et al. (1999) confirm the predominance of surface heating in the mid-latitude North Pacific and the importance of Rossby waves equatorward of 30° latitude in seasonal SSH variability, while the influence of local Ekman pumping is non-negligible in the North Equatorial Current on seasonal timescales. On interannual timescales, the wind-induced first baroclinic mode Rossby waves capture well the large-scale interannual SSH anomaly signals in the 12°–14°N latitudinal band (Qiu and Chen, 2010), while the influence of the eastern boundary forcing appears to be limited to the area a few Rossby radii away from the boundary (Fu and Qiu, 2002). Recently, Piecuch and Ponte (2012) demonstrated that along the southeast tropical Pacific, where the observed patterns of sea level variability are markedly not well correlated with those expected from linear response to wind driving, the buoyancy

* Corresponding author at: Key Laboratory of Coastal Disaster and Defence, Ministry of Education, Hohai University, Nanjing, Jiangsu, China. Tel.: +86 13621581709.
E-mail address: luqinghhu@hotmail.com (Q. Lu).

0921-8181/$ – see front matter © 2013 Elsevier B.V. All rights reserved.
http://dx.doi.org/10.1016/j.gloplacha.2013.04.008

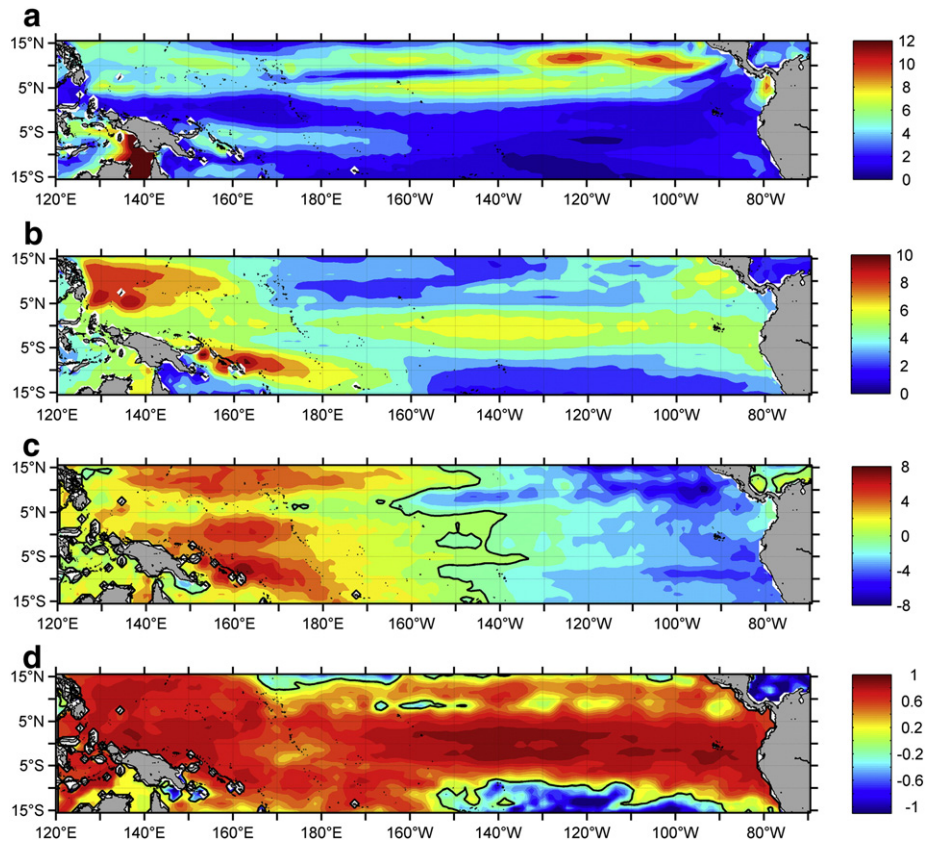

Fig. 1. Components of sea level variability. Standard deviation of (a) seasonal sea surface height (SSH) anomalies (cm), and (b) interannual SSH anomalies (cm). (c) Linear trend in SSH (mm yr^{-1}) over the period 1993–2006 (with the rate of global mean sea level rise removed from the field). (d) Skill of thermosteric expansion above 300 m depth in explaining the variance of altimetry-derived SSH anomalies. Contours indicate a skill of 0.1, black contours denote $S = 0$.

driving plays a crucial role in sea level variability. On low-frequency timescales, the spatial structures of sea level rise in the tropical Pacific Ocean over the last half-century and the past two decades can well be reflected in the thermosteric sea level (Carton et al., 2005; Köhl and Stammer, 2008; Becker et al., 2012). Previous modeling studies have a consensus that the low-frequency changes in the surface wind stress forcing can account for the recent high sea level trends observed in the western tropical Pacific (Köhl and Stammer, 2008; Timmermann et al., 2010; Merrifield and Maltrud, 2011).

However, many recent studies only emphasize the importance of wind forcing in spatially varying sea level trends in the tropical Pacific. A quantitative understanding of the various mechanisms of interannual sea level variability (especially the sea level response to surface heating) is lacking in the tropical Pacific. Our goal in this study is to clarify the contributions of four shallow-water physical processes to interannual sea level variability in the tropical Pacific Ocean. This paper is organized as follows. In the next section, the datasets used in this study are introduced. Section 3 gives a brief description of the observed SSH variability. The contribution of surface heating to interannual sea level variability is presented in Section 4. In Section 5, we discuss the local response to wind forcing. With the aid of a linear 1-1/2-layer reduced-gravity model, the influence of the oceanic large-scale adjustment to wind forcing is described in Section 6. The effects of the eastern boundary forcing are considered in Section 7. Conclusions are given in the final section.

2. Datasets

To understand sea level changes in the tropical Pacific Ocean, we use the global sea surface height anomaly dataset provided by Collecte Localisation Satellite (CLS). The altimeter products were produced by Ssalto/Duacs and distributed by Aviso, with support from CNES (http://www.aviso.oceanobs.com/duacs/). This dataset merges several altimetry measurements, including Topex/Poseidon (T/P), Jason-1 and 2, Envisat and ERS-1 (European Remote Sensing Satellite-1) and 2 (Le Traon et al., 1998; Ducet et al., 2000). It has 1/3° × 1/3° Mercator projection grids at a weekly interval. Because the focus of our study is on the interannual sea level variability, the original weekly SSH anomaly dataset is temporally averaged to form a monthly dataset. To be consistent with the net surface heat flux products and surface wind stress products used in later sections, the altimeter data are interpolated to a 1° × 1° spatial resolution over the time span from January 1993 to December 2006.

Considering that different atmospheric reanalyses have individual biases in their reanalysis fields, and no single reanalysis product is found to agree better in all fields with satellite-derived observations (Chaudhuri et al., 2013), three net surface heat flux products (CORE.2, ECMWF ORA-S3 and OAFlux) and three wind stress products (CORE.2, ECMWF ORA-S3 and SODA) are used to evaluate the contributions of different physical processes to sea level variability. The version 2 of Common Ocean Reference Experiment (CORE.2) Global Air–Sea Flux Dataset (Large and Yeager, 2004) is from the Research Data Archive (RDA) maintained by the Computational and Information Systems Laboratory (CISL). This dataset covers the period from January 1949 through December 2006. The European Centre for Medium-Range Weather Forecasts (ECMWF) operational ocean analysis/reanalysis system (ORA-S3; Balmaseda et al., 2007) is obtained from the Asia–Pacific Data-Research Center (APDRC). Its monthly products are available from January 1959 to December 2009. Two versions of Objectively Analyzed Air–Sea Fluxes (OAFlux; Yu et al., 2008) products can be obtained from the CISL RDA: a daily version (Jan 1985 to Dec 2011) and a monthly

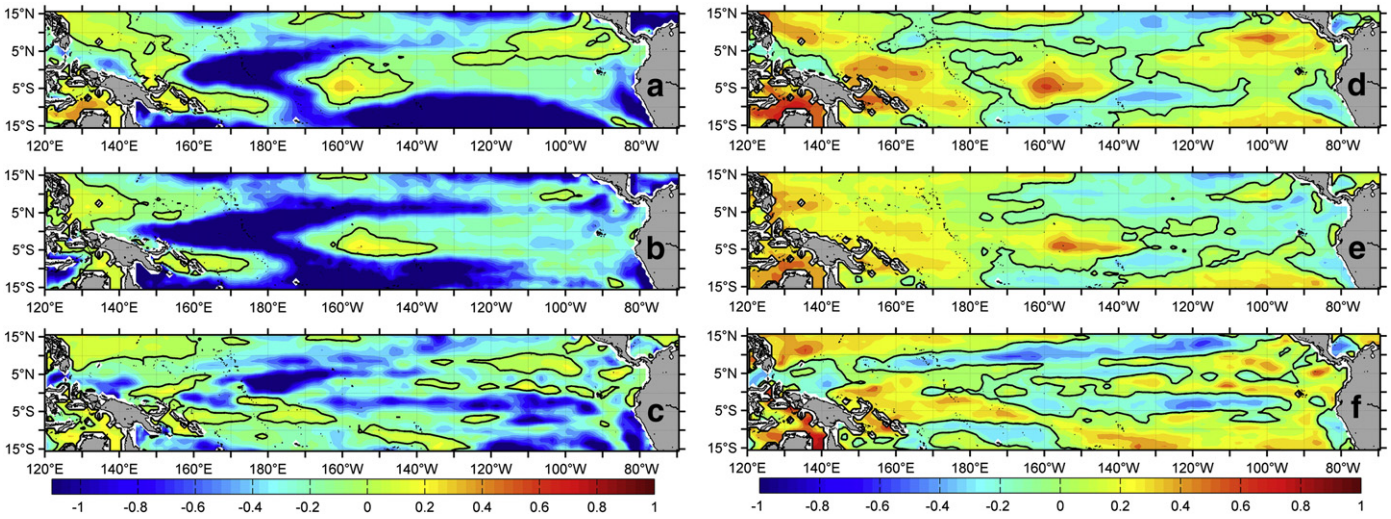

Fig. 2. Skill of local response to surface heating derived from (a) CORE.2, (b) OAFlux, and (c) ECMWF ORA-S3 net surface heat flux products in accounting for the variance of altimetry-derived SSH anomalies. (d), (e), and (f) are the corresponding correlation coefficients between h'_s and observed SSH anomalies. Contours indicate a skill of 0.1, black contours denote $S = 0$.

version (Jan 1958 to Dec 2011). We analyze the monthly version from 1993 to 2006 for our study. The aforementioned three datasets all have a 1° × 1° spatial resolution and a monthly temporal resolution. The Simple Ocean Data Assimilation Reanalysis, version 2.1.6 (SODA 2.1.6; Carton and Giese, 2008) is produced by an ocean general circulation model based on Parallel Ocean Program numerics and is obtained from the International Research Institute for Climate and Society/ Lamont-Doherty Earth Observatory (IRI/LDEO) Climate Data Library. The SODA model run covers the period from 1958 to 2008 and has a horizontal resolution of 0.5° × 0.5° with 40 vertical layers. Its temperature data are also used to calculate the upper ocean thermosteric expansion and heat content.

3. Observed SSH variability

The tropical Pacific Ocean is defined as the area located between 15.5°S and 15.5°N latitude, and 125.5°E and 79.5°W longitude in this study. For the tropical Pacific sea level variability is a superposition of global mean sea level (GMSL) and regional sea level change (Becker et al., 2012; Merrifield et al., 2012), the monthly satellite altimeter GMSL time series from 1993 to 2006, which derived from Church and White (2011), is subtracted from the altimetry-derived SSH signals. In this paper, anomalies of all variables are defined as deviations from the time mean over the period 1993–2006. Interannual anomalies are computed by removing the time mean, seasonal cycle, and linear trend from the monthly time series, then the higher frequency signals with periods < 1 yr are removed from the resulting time series by low-pass filtering.

In the following analyses, we use the predictive skill described by S in Eq. (1) to characterize how well the observed SSH anomaly is represented by the predicted sea level anomaly for a specific physical process. The predictive skill is defined by

$$S = 1 - \frac{\left\langle \left(h_0 - h_p\right)^2 \right\rangle}{\left\langle (h_0)^2 \right\rangle}, \tag{1}$$

where h_0 and h_p are, respectively, the observed SSH anomalies and predicted sea level anomalies, and angle brackets denote time averaging. Predictive skill S ranges between $-\infty$ and 1. High values for predictive skill ($S \to 1$) indicate that observed signal and its prediction are both well correlated and of the same magnitude. Negative values denote that the observation and prediction are out of phase and/or the prediction is larger in magnitude than observation.

Strong seasonal sea level variability is found in the northeastern tropical Pacific (Fig. 1a), where the ratio of the mean seasonal variance to the total sea level variance is higher than 60% (Vinogradov et al., 2008). The standard deviation of interannual sea level variability in the tropical Pacific is shown in Fig. 1b. The strongest interannual sea level signals (6–10 cm) can be found in the off-equatorial western tropical Pacific. Moderate interannual amplitudes (4–5 cm) occur in the equatorial central Pacific and along the American coast. Both seasonal and interannual signals are very weak (<3 cm) in the southeastern tropical Pacific south of 10°S. Sea surface height trends exhibit hemispheric asymmetry in the tropical Pacific for the 1993–2006 period: sea level trends with high rates in the western tropical Pacific, and minimal to negative rates in the eastern tropical Pacific (Fig. 1c).

As the local response to surface heating, local Ekman pumping, wind-induced first baroclinic mode Rossby waves and the eastern boundary forcing are shallow-water physical processes restricted above the thermocline. It is necessary to make sure that these shallow-water physical processes are sufficient to explain sea surface height variability in the tropical Pacific Ocean. Although mass redistribution may be important in shallow, coastal regions (Ponte, 2006) and at high latitudes (Lorbacher et al., 2012), the steric changes arising from ocean temperature variations are the main causes of sea level variability in most regions (Lombard et al., 2009). So thermosteric expansion is calculated as the integral from 0 to 300 m of $\Delta T \alpha dz$. Here α is the thermal expansion coefficient of seawater, which is estimated from the monthly climatologies of temperature and salinity from the World Ocean Atlas 2009 (WOA09; Locarnini et al., 2010; Antonov et al., 2010) averaged over a mixed layer depth, and ΔT is the monthly

Table 1
Predictive skills and correlation coefficients calculated between each of the domain-averaged local responses to surface heating and the corresponding observed SSH anomalies.

	Predictive skill	Correlation coefficient
CORE.2	−1.73	−0.024
OAFlux	−10.75	0.043
ECMWF ORA-S3	−0.30	0.213

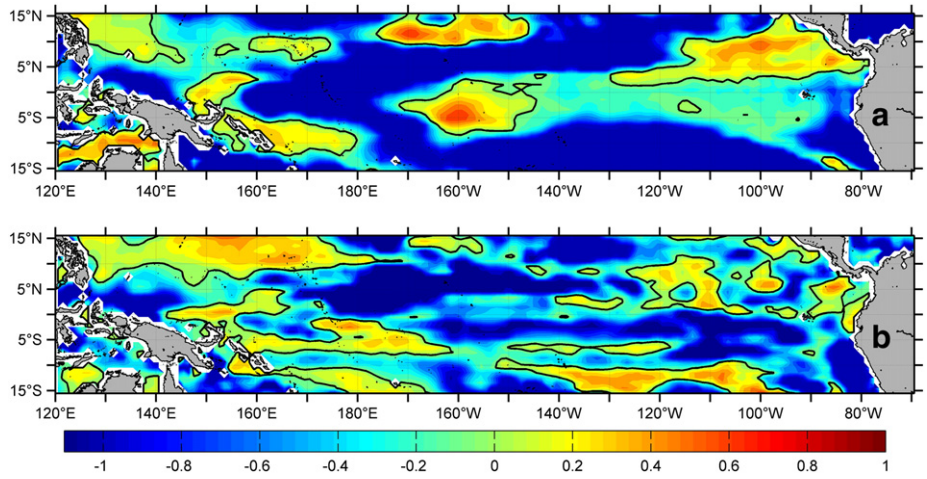

Fig. 3. Skill of local response to surface heating derived from (a) CORE.2, and (b) ECMWF ORA-S3 products in accounting for the interannual variance of altimetry-derived SSH anomalies.

temperature anomaly relative to the 14-year (1993–2006) mean from a multi-year Simple Ocean Data Assimilation (SODA 2.1.6). As shown in Fig. 1d, the thermosteric expansion above the 300 m depth explains at least 60% of the observed sea level variance in the tropical Pacific Ocean, excluding the southeastern tropical Pacific south of 10°S, where the magnitude of the thermosteric expansion variability within the upper ocean is larger than that of the observed sea level variability (not shown). A recent study by Piecuch and Ponte (2011, Fig. 1d) uses the ECCO (Estimating the Circulation and Climate of the Ocean) consortium to provide a sense of the vertical structure of steric sea level. They show that, density changes above 1000 m are able to account for at least 80% of the interannual steric sea level variance in the southeastern tropical Pacific. As indicated in Fig. 1d, the four shallow-water physical processes suffice to explain sea level variability over majority of the tropical Pacific regions, excluding the southeastern tropical Pacific south of 10°S, where deep ocean changes appear to be important.

To investigate more details about interannual SSH variability, two regions with significant interannual sea level changes, as well as with maximal rates of rise are chosen for the subsequent analyses. The geographical extents of the two regions are: the area of 10°–15°N and 130°–155°E in the northwestern tropical Pacific Ocean (defined as NWTP in this paper), as well as the region of 6°–11°S and 160°–175°E in the southwestern Pacific Ocean (defined as SWTP in this paper).

4. Local response to surface heating

As recognized by previous studies, the thermosteric height signals dominate the total steric height changes (e.g., Köhl et al., 2007; Lombard et al., 2009), exceptions are mostly restricted to regions, such as in the Labrador Sea (e.g., Antonov et al., 2002) and the Southern Ocean (e.g., Ponte, 2012). So we neglect the influence of halosteric height signals in the tropical Pacific Ocean. To clarify the contribution of the local thermosteric height anomaly (h'_s) forced by surface heating to sea level variability, we estimate h'_s by using the above-mentioned three net surface heat flux products. The signature of h'_s is determined by integrating

$$\frac{\partial h'_s}{\partial t} = \frac{\alpha(t)}{\rho_0 c_p}\left[Q(t) - \overline{Q(t)}\right], \tag{2}$$

where α, ρ_0, and c_p are the thermal expansion coefficients of seawater, the reference density, and the specific heat, respectively (Vivier et al., 1999; Qiu, 2002). In Eq. (2), $Q(t)$ is the net surface heat flux, and the overbar denotes the temporal average.

The skills of local response to surface heating derived from CORE.2, OAFlux, and ECMWF ORA-S3 net surface heat flux products in accounting for the observed sea level variance are shown in

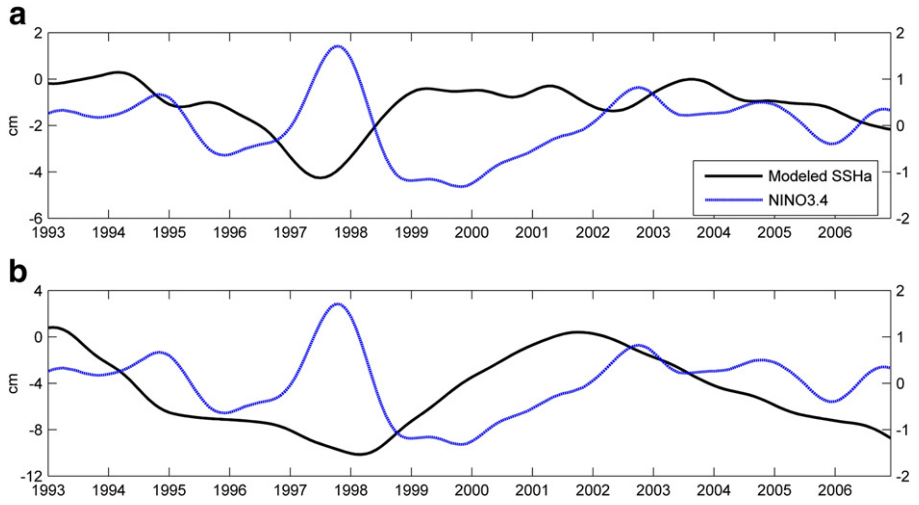

Fig. 4. Time series of the interannual h'_s signals in (a) the NWTP, and (b) the SWTP (black lines). Blue lines denote interannual anomalies of the Niño-3.4 SST index.

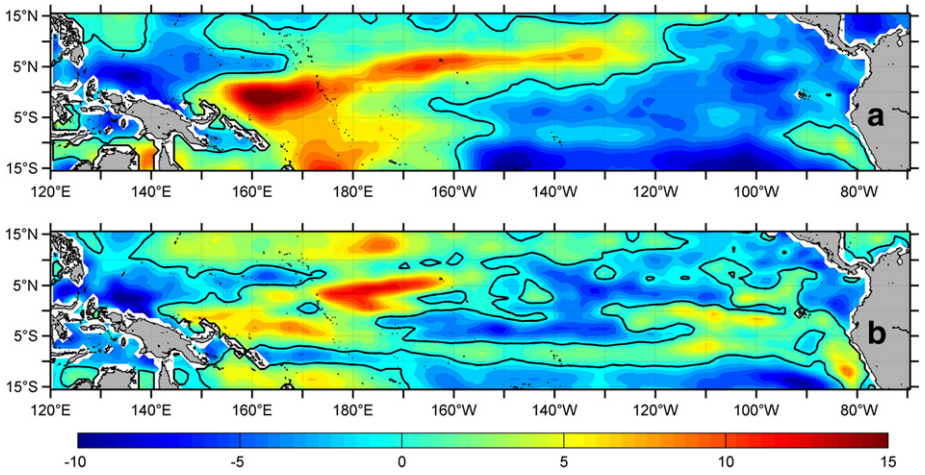

Fig. 5. Linear trend in local response to surface heating (mm yr^{-1}) derived from (a) CORE.2, and (b) ECMWF ORA-S3 products over the period 1993–2006.

Fig. 2a, b, and c, respectively. The correlation coefficients between the observed sea level variability and each of the three local responses to surface heating are also shown in Fig. 2. Regions with positive correlation coefficients and negative predictive skills indicate that the local response to surface heating and observation are out of phase there. Although the two local responses to surface heating forced by CORE.2 and OAFlux products fail to reproduce the observed sea level anomalies along the western equatorial Pacific and in the southern tropical Pacific south of 5°S, they play an important role in reproducing the observed sea level anomalies between the equator and 5°S, around 160°W, while the h'_s forced by ECMWF ORA-S3 surface heating does not exhibit any contribution to SSH variability in this region. Given the different predictive skill spatial patterns of the three local responses to surface heating, it is not easy to make an assessment which product is the best/worst one to reproduce the observed SSH variability. So each of the three domain-averaged thermosteric height anomaly (h'_s) signals deduced from the three net surface heat flux products is then compared with the observed SSH anomalies averaged in the same region, based on the correlation and predictive skill (see Table 1). The tropical Pacific Ocean, excluding the region of 8.5°–15.5°S and 155.5°W–79.5°W, is defined as the domain in this study. As the predictive skills listed in Table 1, although all three h'_s signals are out of phase with the observed SSH anomalies, the h'_s forced by the OAFlux product is inferior to the CORE.2 and ECMWF ORA-S3 forced simulations in reproducing sea level variability in the tropical Pacific because the magnitude of h'_s forced by the OAFlux product is much larger than that of the observation.

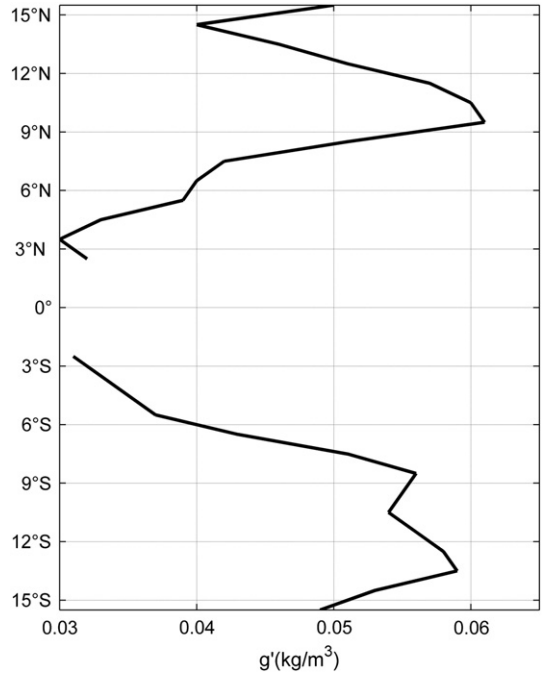

Fig. 6. Latitude-specifics of reduced gravity value g'.

The skills of h'_s derived from CORE.2 and ECMWF ORA-S3 products in accounting for the interannual variance of altimetry-derived SSH anomalies are shown in Fig. 3. There are various differences in these two interannual predictive skill spatial patterns. As such, we do not think that any specific net surface heat flux product can reproduce the most observed interannual SSH variability in the tropical Pacific Ocean. The choice of net surface heat flux product can have an obvious effect on the interpretation of interannual sea level variability in some regions, such as in the northwestern tropical Pacific and the equatorial central Pacific. As shown in Fig. 3, it is clear that both of the two local responses to surface heating make a contribution, which cannot be ignored, to interannual sea level anomalies in the northeastern tropical Pacific (h'_s accounts for 20%–60% of the interannual variance) and the western equatorial Pacific around 150°E (h'_s accounts for 20%–50% of the interannual variance), but the h'_s forced by the ECMWF ORA-S3 product is better in explaining interannual sea level variability in the northwestern tropical Pacific and the southeastern tropical Pacific south of 10°S, while the h'_s derived from the CORE.2 product is better in reproducing interannual SSH anomalies in the southwestern tropical Pacific near the Solomon Islands and the central tropical Pacific around 160°W. Fig. 4a and b show the time series of h'_s averaged in the NWTP and SWTP, which are forced by ECMWF ORA-S3 and CORE.2 products, respectively. As the El Niño-Southern Oscillations (ENSO) variability, especially during the 97/98 El Niño event over the studied period, is the strongest interannual signal in the tropical Pacific Ocean, the Niño-3.4 (5°S–5°N, 170°W–120°W) SST index is used to represent the ENSO variability in this study (Fig. 4). Here the time mean, seasonal cycle, linear trend, and the higher frequency signals with periods < 1 yr are also removed from the Niño-3.4 SST index. The maximum correlation reaches −0.71 with h'_s in the NWTP leading the Niño-3.4 SST index by 1 month during the 97/98 El Niño event, whereas the maximum correlation between the SWTP h'_s and the Niño-3.4 SST index is −0.68 with a 6-month lag. The correlation relations suggest that the turnabout of interannual net surface heat flux anomalies from a cold phase to a warm phase in the NWTP is earlier than that in the SWTP during the 97/98 El Niño event. Considering that net surface heat flux is the outcome of ocean–atmosphere interaction, which is beyond the scope of this study,

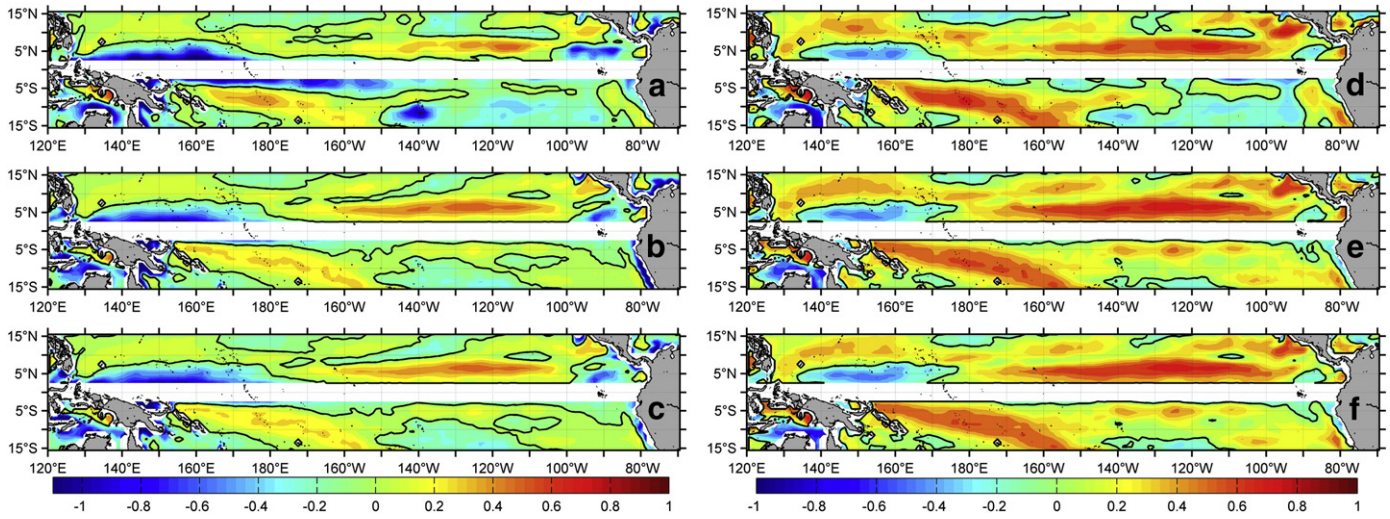

Fig. 7. Skill of local response to wind forcing derived from (a) CORE.2, (b) SODA 2.1.6, and (c) ECMWF ORA-S3 wind stress products in accounting for the variance of altimetry-derived SSH anomalies. (d), (e), and (f) are the corresponding correlation coefficients between h'_{EK} and observed SSH anomalies. Contours indicate a skill of 0.1, black contours denote $S = 0$.

the reason why the net surface heat fluxes in the above-mentioned two regions are out of phase will not be discussed in this paper.

Although there are various differences in the interannual predictive skill spatial patterns of local response to surface heating derived from CORE.2 and ECMWF ORA-S3 products, the spatial patterns of the linear trend in the two local responses to surface heating are more similar (Fig. 5). There is a robust positive trend in the local response to surface heating (also exists in the h'_s forced by OAFlux net surface heat flux, not shown) along the western equatorial Pacific (150°–180°E) that appears to explain the large (about 1 cm/yr) altimetry-derived sea level trend in this region. The different magnitudes of trend shown in Fig. 5a and b may be attributed to the individual biases in respective reanalysis fields (Chaudhuri et al., 2013). However, the positive trend along the western equatorial Pacific is not reproduced in several contemporary studies (e.g., Timmermann et al., 2010, Fig. 2c; Qiu and Chen, 2012, Fig. 10b), because linear trends in the tropical Pacific in these studies are only wind-driven, other forcing mechanisms are ignored.

Although local changes in net surface heat flux show some skill in explaining the interannual sea level variability, we expect that the lack of ocean dynamics, such as local Ekman pumping and wind-induced first baroclinic mode Rossby waves, is the cause for the poor contribution in the deep blue regions shown in Fig. 3. These dynamic processes will be explored in the subsequent analyses.

5. Local response to wind forcing

Apart from the local influence of surface heating, the effect of the oceanic local response to wind forcing on SSH anomalies is governed by Ekman dynamic. Wind stress curl anomalies cause changes in the convergence of near-surface Ekman transports. Depending on the sign of the related Ekman pumping velocity, warm (cold) water is pumped down (sucked up), which leads to a deepening (shoaling) of the thermocline and a local sea level increase (decrease). The Ekman pumping has been used to quantify the oceanic local response to wind forcing on seasonal timescales (Vivier et al., 1999) and interannual timescales in a two-layer model (Qiu, 2002). Specifically,

$$\frac{\partial h'_{EK}}{\partial t} = -\frac{g'}{\rho_0 g}\,\mathrm{curl}\left(\frac{\tau}{f}\right), \tag{3}$$

where h'_{EK} is the Ekman-dynamical height anomaly, g' is the reduced gravity, f is the Coriolis parameter, and τ is the anomalous wind stress vector. The value of g' reflects the strength of stratification, it does control the magnitude of h'_{EK}, but does not influence the pattern of the h'_{EK} field. In order to obtain the suitable g', following the studies of the tropical Pacific by Timmermann et al. (2010) and McGregor et al. (2012) with a linear reduced-gravity shallow-water model (SWM), we prescribe the reduced-gravity parameter $g'_{SW} = 0.05\ \mathrm{m\ s^{-2}}$ in this study, which is constant in space and time. Replacing g' with g'_{SW} in Eq. (3), we get h'_{SW}. Linear regression coefficients ($\gamma(x,y)$) are calculated at each grid point between the observed SSH variability and the h'_{SW} driven by each of the three aforementioned wind stress products. This results in three separate regression coefficient fields, and then the average of these three regression coefficient fields is calculated. There are more robust meridional features than zonal features in the average regression coefficient field (Timmermann et al., 2010; McGregor et al., 2012), so the latitudinal mean of the average regression field is used to calculate $g'\left(g' = \overline{\gamma}(y)g'_{SW}\right)$. Fig. 6 shows the latitude-varying g' values. There are local minimal g' values along 4°N and 14°N and local maximal g' values along 10°N, corresponding to the thermocline troughs and ridge, respectively (Wang et al., 2000; Kessler, 2002).

The skills of local Ekman pumping in accounting for the observed SSH variance are shown in Fig. 7a, b, and c, corresponding to wind

Table 2
Predictive skills and correlation coefficients calculated between each of the domain-averaged local responses to wind forcing and the corresponding observed SSH anomalies.

	Predictive skill	Correlation coefficient
CORE.2	−0.40	−0.120
SODA 2.1.6	−0.17	0.043
ECMWF ORA-S3	−0.17	0.049

Table 3
Predictive skills and correlation coefficients calculated between each of the domain-averaged wind-induced first baroclinic mode Rossby waves and the corresponding observed SSH anomalies.

	Predictive skill	Correlation coefficient
CORE.2	0.28	0.554
SODA 2.1.6	0.45	0.668
ECMWF ORA-S3	0.43	0.661

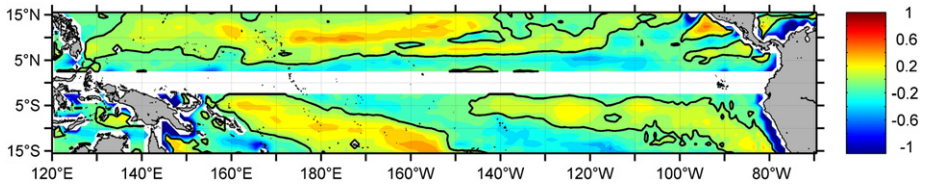

Fig. 8. Skill of local response to wind forcing derived from SODA 2.1.6 in accounting for the interannual variance of altimetry-derived SSH anomalies.

stress forcing from CORE.2, SODA, and ECMWF ORA-S3, respectively. The correlation coefficients between the observed sea level variability and each of the three local responses to wind forcing are also shown in Fig. 7. Relative to h'_s, the predictive skill spatial patterns of h'_{EK} are more comparable to each other because of the wind products' similar physical assumptions and assimilation of common observations (Chaudhuri et al., 2013). Remarkable fraction of the altimetry-derived SSH variance can be explained by local Ekman pumping between 5°N and 10°N in the northeastern tropical Pacific, extending from 170°W to 100°W (h'_{EK} accounts for 20%–60% of the total variance). It is also found that local Ekman pumping plays an important role in regulating the seasonal meridional movement of the North Equatorial Countercurrent (NECC) Center (Hsin and Qiu, 2012) in this region. The contribution of local Ekman pumping to the observed SSH variability in the southwestern tropical Pacific also cannot be ignored (h'_{EK} accounts for 20%–40% of the total variance).

In the tropical Pacific Ocean, the skill of h'_{EK} derived from the CORE.2 wind stress product is weaker in accounting for the observed SSH variance than those derived from SODA and ECMWF ORA-S3 wind stress products (see Fig. 7a and d, and Table 2). Although the predictive skills of domain-averaged h'_{EK} derived from SODA and ECMWF ORA-S3 wind stress products are very close (listed in Table 2), the first baroclinic mode Rossby waves driven by SODA wind stress are better in reproducing the observed SSH anomalies than those driven by ECMWF ORA-S3 wind stress (see Fig. 12 and Table 3). So we use the h'_{EK} driven by SODA wind stress for the subsequent analyses.

The contribution of local Ekman pumping to interannual SSH variability is notable in the area of 170°E–150°W around 10°N, the coastal region of Nicaragua, and the southwestern tropical Pacific (h'_{EK} accounts for 20%–60% of the interannual variance, shown in Fig. 8). Whereas, local Ekman pumping dynamic poorly explains the interannual variability of observed SSH anomalies (h'_{EK} accounts for less than 30% of the interannual variance) in the eastern tropical Pacific characterized by positive SST anomalies during the 97/98 El Niño event, which indicates that El Niño warming in this region is not the result of local change in surface wind forcing (Wyrtki, 1975). To analyze the detailed interannual variability of observed SSH anomalies, the time series of h'_{EK} averaged in the NWTP and SWTP are plotted in Fig. 9a and b, respectively. An overall good correspondence between h'_{EK} and the Niño-3.4 SST index is easily discernible. The maximum correlation of -0.81 occurs with h'_{EK} in the NWTP leading the Niño-3.4 SST index by 6 months, whereas the maximum correlation between the SWTP h'_{EK} and the Niño-3.4 SST index is -0.90 with a zero month lag. As there is a close relationship between wind stress anomaly and local Ekman pumping response, the above correlation relations indicate that the off-equatorial cyclone in the NWTP decays earlier than that in the SWTP during El Niño. Condensation heating in the equatorial central Pacific (Zebiak, 1990; Weisberg and Wang, 1997) induces a pair of off-equatorial cyclones, and then the off-equatorial cyclones raise the thermocline there via local Ekman pumping. The shallow off-equatorial thermocline anomaly expanding over the western Pacific leads to an increase in sea level pressure (SLP) and an anomalous anticyclone in the NWTP (e.g. Wang, 2000), while the SWTP is still controlled by the off-equatorial cyclone. So there is a lag between the SWTP h'_{EK} and NWTP h'_{EK} during El Niño. However, the magnitude of h'_{EK} in the SWTP is almost twice as large as that in the NWTP, which indicates that the wind stress in the SWTP is stronger in strength than in the NWTP.

6. Wind-induced baroclinic Rossby waves

In the tropical Pacific Ocean, SSH variability is predominantly induced by the time-varying surface wind forcing (Köhl and Stammer, 2008; Timmermann et al., 2010; McGregor et al., 2012). The 1-1/2-layer reduced-gravity model has been used to quantify the wind-induced SSH variability in many past studies (e.g., Meyers, 1979; Kessler, 1990; Qiu

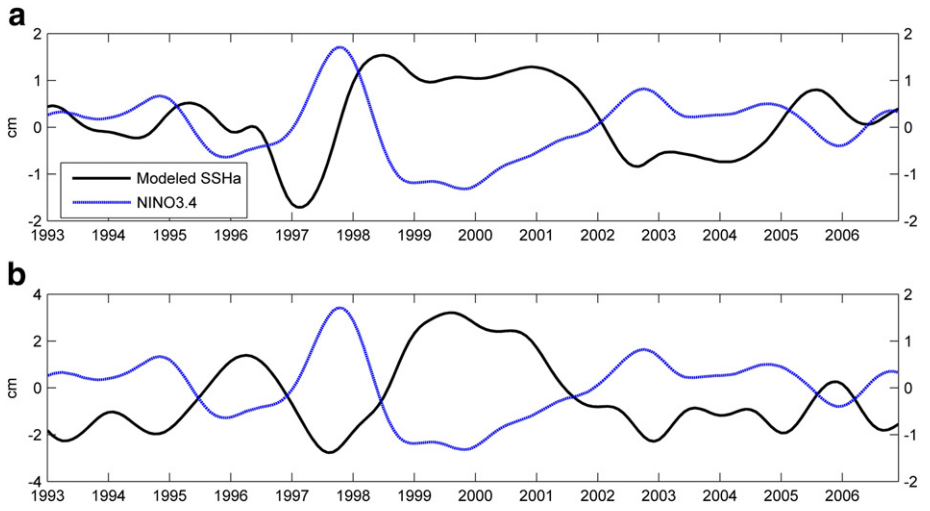

Fig. 9. Time series of the interannual h'_{EK} signals in (a) the NWTP, and (b) the SWTP (black lines). Blue lines denote interannual anomalies of the Niño-3.4 SST index.

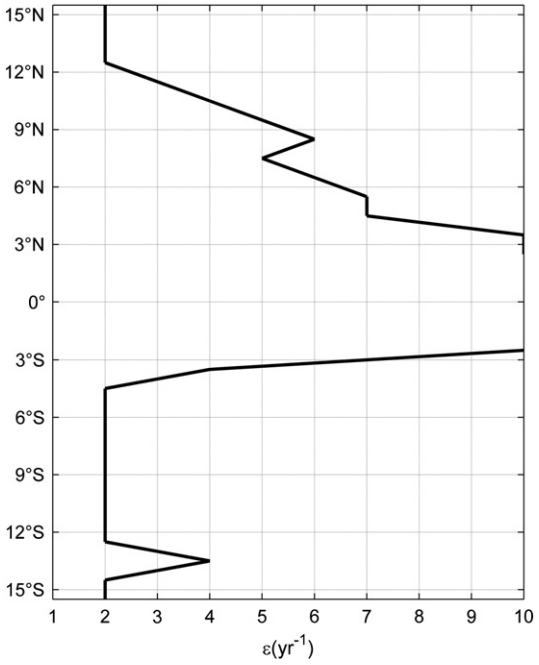

Fig. 10. Latitude-specifics of Newtonian dissipation rate ε.

and Joyce, 1992; Capotondi and Alexander, 2001; Qiu and Chen, 2006). Under the long-wave approximation, a linear vorticity equation (with zero background flow) governing the 1-1/2-layer reduced-gravity model is given by

$$\frac{\partial h'}{\partial t} - C_R \frac{\partial h'}{\partial x} = -\frac{g' \nabla \times \tau}{g \rho_0 f} - \varepsilon h', \tag{4}$$

where $h'(x,y,t)$ is the SSH anomaly, $C_R(x,y) = \beta(y) C_1(x,y)^2 / f(y)^2$ is the phase speed of the first baroclinic mode Rossby waves, $\beta(y)$ is the meridional derivative of the Coriolis parameter, $C_1(x,y)$ is the phase speed of the first baroclinic mode gravity wave, and ε is the Newtonian dissipation rate. By integrating Eq. (4) from the eastern boundary ($x = x_e$) along the baroclinic Rossby wave characteristic, h' has an analytic solution of

$$h'_m(x,y,t) = \frac{g'}{\rho_0 g f} \int_{x_e}^{x} \frac{1}{C_R} \nabla \times \tau \left(x', y, t + \frac{x - x'}{C_R} \right) \times \exp\left[\frac{\varepsilon}{C_R} (x - x') \right] dx', \tag{5}$$

where h'_m is the modeled SSH anomaly deduced from the wind-driven, linear 1-1/2-layer reduced-gravity model. According to Fu and Qiu (2002), the influence of the eastern boundary on sea level variability is limited to a narrow area within a few Rossby radii away from the boundary, thus the solution due to the eastern boundary forcing has been ignored in Eq. (5).

The wind forcing data used in Eq. (5) are the same monthly wind stress products as used in Section 5. The baroclinic Rossby wave speed C_R is evaluated from the global climatological first baroclinic mode gravity-wave phase speed $C_1(x,y)$ derived by Chelton et al. (1998). At the latitude of about 15°N, the C_R values vary from 0.1 m s^{-1} in the eastern basin to 0.17 m s^{-1} in the western basin, and these values indicate about a 3 yr transit time required by a long baroclinic Rossby wave to cross the Tropical Pacific basin.

When ρ_0, g' and other parameters are given, h'_m has a complicated dependence on ε. Since the ε value is a poorly known quantity, we follow Qiu (2002) to calculate the h'_m signals using a wide range of the ε values (ε = 0.5, 1–10 yr^{-1}), and then choose the optimal dissipation rate corresponding to the maximum predictive skill at each grid point. Three wind stress products result in three separate fields of dissipation rates. In calculating the h'_m signals, it would be ideal to use the mean value of three dissipation rate fields derived from the three wind stress products. Since there are more robust meridional features than zonal features in the average dissipation rate field, we run the linear vorticity model by inputting the latitudinal averaged dissipation rates shown in Fig. 10.

As shown in Fig. 11a, b, and c, the contribution of wind-induced first baroclinic mode Rossby waves to the observed SSH anomalies is predominant in the tropical Pacific (h'_m accounts for 30%–80% of the total variance). It is worth to notice that the predictive skill of h'_m drops rather rapidly from 10°N toward the equator in the west of 170°E, where the Mindanao Eddy and the Halmahera Eddy are located, as investigated by Tozuka et al. (2001). Another region is the southeastern tropical Pacific south of 10°S, where the wind-

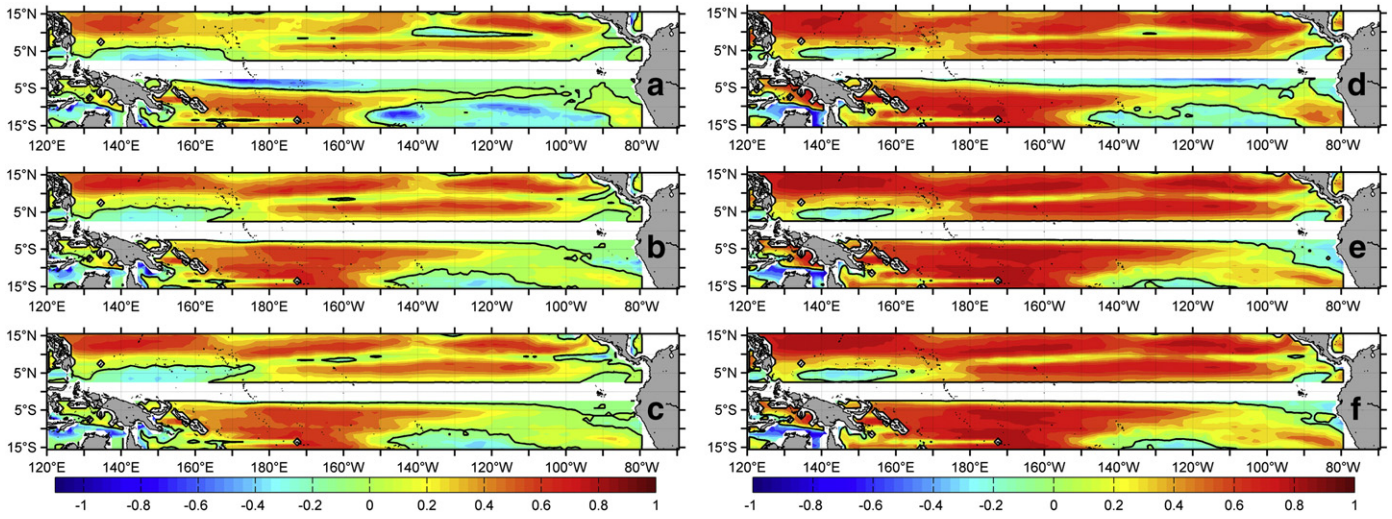

Fig. 11. Skill of wind-induced first baroclinic mode Rossby waves driven by (a) CORE.2, (b) SODA 2.1.6, and (c) ECMWF ORA-S3 wind stress products in accounting for the variance of altimetry-derived SSH anomalies. (d), (e), and (f) are the corresponding correlation coefficients between h'_m and observed SSH anomalies. Contours indicate a skill of 0.1, black contours denote $S = 0$.

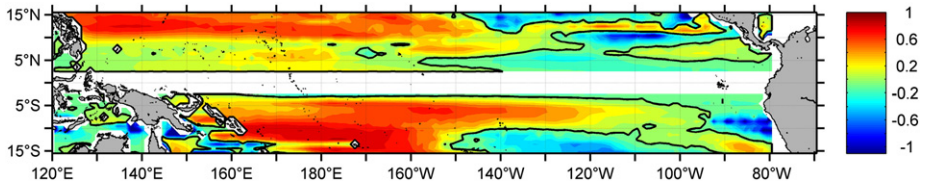

Fig. 12. Skill of wind-induced first baroclinic mode Rossby waves driven by SODA 2.1.6 wind stress product in accounting for the interannual variance of altimetry-derived SSH anomalies.

induced first baroclinic mode Rossby waves poorly explain the observed SSH variance, and the variability within the deep ocean cannot be overlooked. Although there are high correlations between each of the three wind stress forced simulations and the observed SSH anomalies (shown in Fig. 11d, e, and f), the skill of h'_m derived from CORE.2 wind stress is inferior in accounting for the observed sea level variance to those derived from SODA and ECMWF ORA-S3 wind stress products (see Fig. 11a, b, and c), particularly in the southern tropical Pacific. Considering that the two predictive skill spatial patterns of h'_m derived from SODA and ECMWF ORA-S3 wind stress products are very similar, the domain-averaged h'_m is used to compare predictive skills (see Table 3). The h'_m forced by SODA wind stress is better in both predictive skill and correlation coefficient than that driven by ECMWF ORA-S3 wind stress, so the h'_m driven by SODA wind stress is chosen to analyze the contribution of wind-induced first baroclinic mode Rossby waves to interannual variability of altimetry-derived SSH anomalies (shown in Fig. 12).

The wind-induced first baroclinic mode Rossby waves play a predominant role in interannual sea level change in the western tropical Pacific, while the contribution of h'_m to interannual SSH variability is relatively weak in the eastern tropical Pacific, especially along the South American coast. Time series of h'_m in the NWTP and SWTP are shown in Fig. 13a and b. An overall good correspondence between h'_m and the Niño-3.4 SST index is easily discernible. The maximum correlation of -0.82 occurs with h'_m in the NWTP leading the Niño-3.4 SST index by 2 months, whereas the maximum correlation between the SWTP h'_m and the Niño-3.4 SST index is -0.75 with a 4-month lag. Because the changes in h'_m reflect the accumulative effect of the time-varying wind forcing along the Rossby wave characteristics across the tropical Pacific basin, the above correlations suggest that the changes in wind stress in the 10°–15°N latitudinal band leads that in the 6°–11°S latitudinal band.

7. Effects of the eastern boundary forcing

As shown in Figs. 8 and 12, the wind-driven dynamics are not sufficient to explain the observed interannual SSH anomalies in the eastern tropical Pacific, especially along the South American coast. Since the influence of the eastern boundary forcing is crucial for explaining the observed SSH anomalies along the American coast (Fu and Qiu, 2002; Qiu and Chen, 2006), the effects of eastern boundary forcing are considered in this section. Specifically,

$$h'_e(x,y,t) = h\left(x_e, y, t + \frac{x - x_e}{C_R}\right) \exp\left[\frac{\varepsilon_B}{C_R}(x - x_e)\right], \tag{6}$$

where h'_e is the eastern boundary forced SSH anomaly, and ε_B is the Newtonian dissipation rate associated with the boundary-forced signals. The value of ε_B is affected by the vertical propagation of wave energy into the subthermocline and topographic scattering (Kessler and McCreary, 1993). Following the studies of the eastern South Pacific by Vega et al. (2003) and Qiu and Chen (2006), $\varepsilon_B = (300\ \text{days})^{-1}$ is adopted in this study. Also, we follow Fu and Qiu (2002) to regard the monthly altimetry-derived SSH signals next to the coast as $h(x_e,y,t)$.

Fig. 14 shows the contribution of the eastern boundary forced signals to the observed interannual SSH anomalies. It shows clearly that on interannual timescales, the eastern boundary forcing is dominant (h'_e accounts for 20%–70% of the interannual variance) in the east of 120°W between 10°N and 10°S. Besides, the effect of the eastern boundary forcing in the eastern tropical South Pacific is stronger than that in the eastern tropical North Pacific, where the contributions of local surface heating and local Ekman pumping cannot be overlooked. This implies that the 97/98 El Niño warming along the South American coast is not the result of local change in wind forcing,

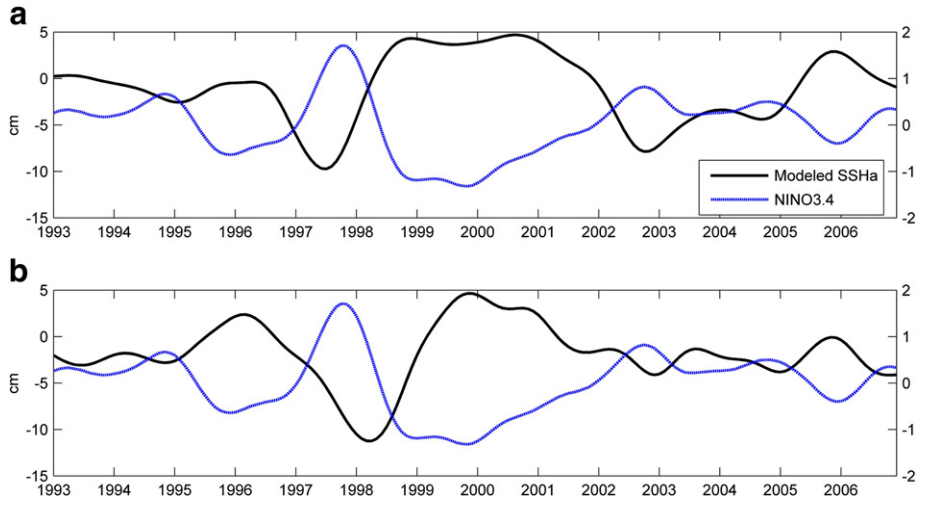

Fig. 13. Time series of the interannual h'_m signals in (a) the NWTP, and (b) the SWTP (black lines). Blue lines denote interannual anomalies of the Niño-3.4 SST index.

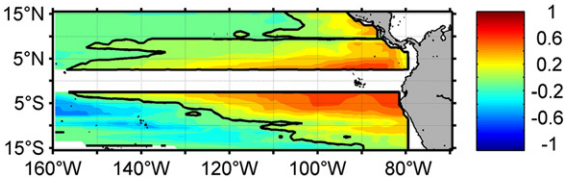

Fig. 14. Skill of the eastern boundary forcing in accounting for the interannual variance of altimetry-derived SSH anomalies.

but rather reflects a remote response to the rapidly decreased easterly trade wind in the equatorial central Pacific (Wyrtki, 1975). To gain an insight into the remote response, Fig. 15 shows the time-longitude plot of upper ocean heat content in the 2°N–2°S latitudinal band and the time–latitude plots of upper ocean heat content along the South and North American coast. Here heat content is calculated as the integral from 0 to 300 m of $\rho c_p T(z)dz$, the temperature data are from SODA 2.1.6. It is clear that there is a strong eastward heat content signal during the 97/98 El Niño event, and the heat content transporting along the South American coast is larger in magnitude than that transporting along the North American coast.

8. Summary and conclusions

Altimetry-derived sea surface height data over the period 1993–2006 are used to investigate the interannual SSH variability in the tropical Pacific Ocean. The significant interannual SSH signals are found in the northwestern tropical Pacific and southwestern tropical Pacific. The thermosteric height variability within the upper 300 m ocean accounts for >60% of SSH variance in the tropical Pacific, excluding the southeastern tropical Pacific south of 10°S, where deep ocean variability cannot be overlooked. So the shallow-water processes are sufficient to explain the observed SSH variability in the tropical Pacific.

We must consider that each reanalysis product has individual bias, and no single reanalysis product is found to agree well in all fields with satellite-derived observations (Chaudhuri et al., 2013). Three net surface heat flux products and three wind stress products are used to investigate the local response to surface heating and the oceanic responses to wind forcing, respectively.

The surface heating from OAFlux is inferior in reproducing observed sea level anomalies to that from CORE.2 and ECMWF ORA-S3 in the tropical Pacific because the h_s' (local thermosteric height anomaly

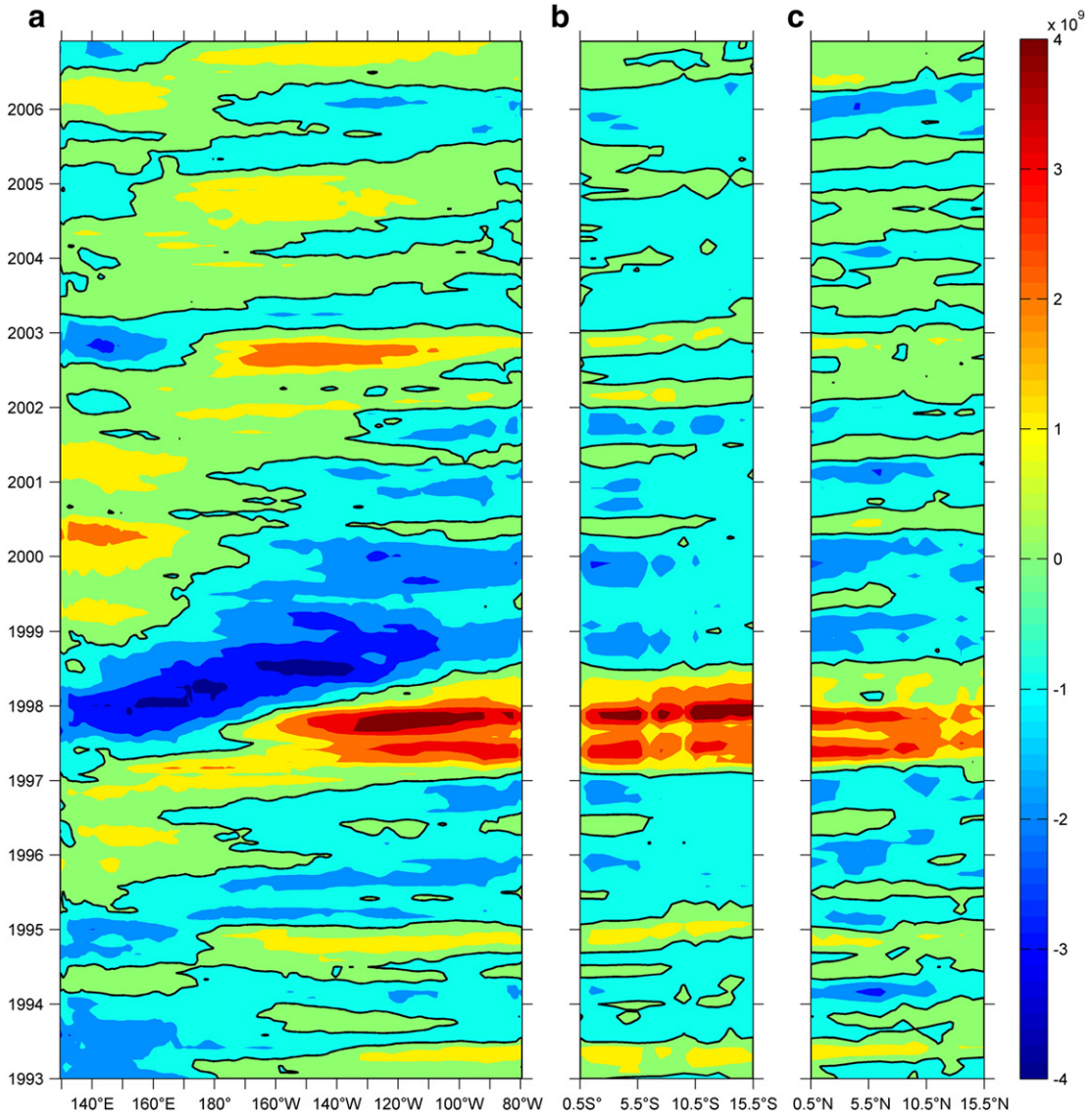

Fig. 15. (a) Time-longitude plot of the heat content anomalies (J m^{-2}) in the 2°N–2°S latitudinal band, and time–latitude plots of the heat content anomalies along (b) the South American coast, and (c) the North American coast.

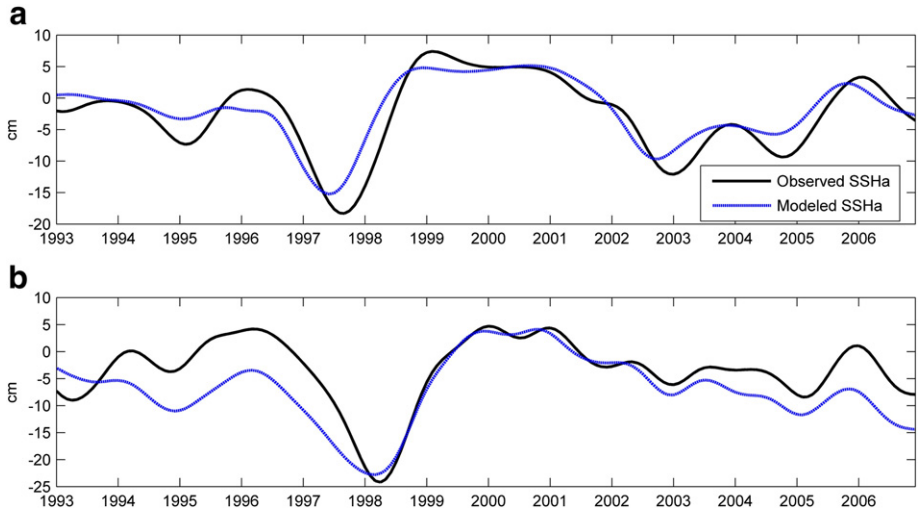

Fig. 16. Time series of the interannual SSH anomalies obtained from the satellite altimeter measurements (black lines) and the sum of h'_s, h'_{EK}, and h'_m (blue lines) in (a) the NWTP, and (b) the SWTP.

to surface heating) forced by the OAFlux product is much larger in magnitude than the observation. Considering that there are various differences in the two interannual predictive skill spatial patterns of h'_s derived from CORE.2 and ECMWF ORA-S3 products, we do not think that any specific net surface heat flux product can reproduce the most observed interannual SSH variability in the tropical Pacific Ocean. The choice of surface heating product has an obvious effect on the interpretation of interannual sea level variability in some regions, such as in the northwestern tropical Pacific and the equatorial central Pacific.

Although there are various differences in the interannual predictive skill spatial patterns of h'_s derived from CORE.2 and ECMWF ORA-S3 products, the spatial patterns of linear trend in the two local responses to surface heating are more similar (Fig. 5). There is a robust positive trend in local response to surface heating along the western equatorial Pacific (150°–180°E) that appears to explain the large (about 1 cm/yr) altimetry-derived sea level trend in this region. The different magnitudes of trend may be attributed to the individual biases in respective reanalysis fields (Chaudhuri et al., 2013). However, the positive trend along the equatorial western Pacific is not reproduced in several contemporary studies (e.g., Timmermann et al., 2010, Fig. 2c; Qiu and Chen, 2012, Fig. 10b), because only a wind-driving mechanism is considered to calculate the linear trends of the tropical Pacific SSH anomaly, other forcing mechanisms are ignored in these studies.

Relative to h'_s, the predictive skill spatial patterns of h'_{EK} or h'_m are more comparable because of the wind products' similar physical assumptions and assimilation of common observations (Chaudhuri et al., 2013). The CORE.2 wind stress is inferior in reproducing the observed SSH anomalies to the other two wind stress products in the tropical Pacific, especially in the tropical South Pacific. The h'_m driven by SODA wind stress is a little better in accounting for the observed sea level variance than that driven by ECMWF ORA-S3 wind stress in the tropical Pacific basin.

The dominant processes affecting interannual variability of observed SSH anomalies vary regionally in the tropical Pacific; local response to surface heating, local Ekman pumping, wind-induced first baroclinic mode Rossby waves and the eastern boundary forcing are all important. Both the local response to surface heating and the eastern boundary forcing are important in explaining the interannual variance of observed SSH anomalies in the northeastern tropical Pacific; while the interannual SSH variability in the southeastern tropical Pacific is dominated by the eastern boundary forcing, the local Ekman pumping plays a relatively minor role in the interannual SSH change. The different contributions of local response to surface heating to interannual sea level variability in the eastern tropical North and South Pacific imply that the ocean–atmosphere interaction in the northeastern tropical Pacific is more active than that in the southeastern tropical Pacific. As the 97/98 El Niño is the strongest interannual signal over the studied period, all of these suggest that the 97/98 El Niño warming along the South American coast is not the result of local change in wind forcing, but rather reflects a remote response to the rapidly decreased easterly trade wind in the equatorial central Pacific (Wyrtki, 1975). In addition, the local response to surface heating also plays an important role in accounting for the interannual SSH variance in the southeastern tropical Pacific south of 10°S, where deep ocean variability cannot be overlooked.

The wind-induced first baroclinic mode Rossby waves dominate interannual SSH variability in the western tropical Pacific, excluding the area of 2°–10°N, west of 170°E, where the Mindanao Eddy and the Halmahera Eddy are located (Tozuka et al., 2001) and the linear 1-1/2-layer reduced-gravity dynamic is inadequate. Although a large part of the interannual sea level variability in the western tropical Pacific is related to the oceanic remote adjustment to wind stress forcing, the contributions of local responses to surface heating and wind forcing cannot be overlooked.

Comparing the time series of h'_s and h'_{EK} with the Niño-3.4 SST index, we find that the change in both h'_s and h'_{EK} signals in the NWTP lead that in Niño-3.4 SST, whereas the corresponding change in the SWTP lag that in Niño-3.4 SST during the 97/98 El Niño. This lead–lag relationship during the ENSO event may associate with the strong ocean–atmosphere interaction in the equatorial central Pacific. The total interannual sea level time series, which contain h'_s, h'_{EK}, and h'_m signals, in the NWTP and SWTP are shown in Fig. 16a and b (blue lines), respectively. As shown in Fig. 16, the three shallow-water processes are sufficient to explain the interannual variance of altimetry-derived SSH anomalies, and the differences between the sum of the three simulations and the observation may be attributed to the nonlinear effects and the biases of those forcing products.

Acknowledgements

This research is supported by the National Natural Science Foundation of China (Grant No. 41276018), the Major Project of Chinese National Programs for Fundamental Research and Development (973 Program No. 2013CB430302), and the Program Sponsored for Innovation Research of Graduate Student in Jiangsu Province, China (Grant No. CXZZ11_0422). We thank the two anonymous reviewers for their very helpful comments.

References

Antonov, J.I., Levitus, S., Boyer, T.P., 2002. Steric sea level variations during 1957–1994: importance of salinity. Journal of Geophysical Research 107 (C12), 8013. http://dx.doi.org/10.1029/2001JC000964.

Antonov, J.I., Seidov, D., Boyer, T.P., Locarnini, R.A., Mishonov, A.V., Garcia, H.E., Baranova, O.K., Zweng, M.M., Johnson, D.R., 2010. World ocean atlas 2009, volume 2: salinity. In: Levitus, S. (Ed.), NOAA Atlas NESDIS 69. U.S. Government Printing Office, Washington, D.C. (184 pp.).

Balmaseda, M.A., Vidard, A., Anderson, D.L.T., 2007. The ECMWF ocean analysis system: ORA-S3. Monthly Weather Review 136, 3018–3034.

Becker, M., Meyssignac, B., Letetrel, C., Llovel, W., Cazenave, A., Delcroix, T., 2012. Sea level variations at tropical Pacific islands since 1950. Global and Planetary Change 85–98. http://dx.doi.org/10.1016/j.gloplacha.2011.09.004.

Capotondi, A., Alexander, M.A., 2001. Rossby waves in the tropical North Pacific and their role in decadal thermocline variability. Journal of Physical Oceanography 31, 3496–3515.

Carton, James A., Giese, Benjamin S., 2008. A Reanalysis of ocean climate using Simple Ocean Data Assimilation (SODA). Monthly Weather Review 136, 2999–3017. http://dx.doi.org/10.1175/2007MWR1978.1.

Carton, J.A., Giese, B.S., Grodsky, S.A., 2005. Sea level and the warming of the oceans in the Simple Ocean Data Assimilation (SODA) ocean reanalysis. Journal of Geophysical Research 110, C09006. http://dx.doi.org/10.1029/2004JC002817.

Chaudhuri, Ayan H., Ponte, Rui M., Forget, Gael, Heimbach, Patrick, 2013. A comparison of atmospheric reanalysis surface products over the ocean and implications for uncertainties in air–sea boundary forcing. Journal of Climate 26, 153–170. http://dx.doi.org/10.1175/JCLI-D-12-00090.1.

Chelton, D.B., de Szoeke, R.A., Schlax, M.G., Naggar, K.E., Siwertz, N., 1998. Geographical variability of the first baroclinic Rossby radius of deformation. Journal of Physical Oceanography 28, 433–460. http://dx.doi.org/10.1175/1520-0485(1998)028<0433:GVOTFB>2.0.CO;2.

Church, J.A., White, N.J., 2011. Sea-level rise from the late 19th to the early 21st century. Surveys in Geophysics 32, 585–602. http://dx.doi.org/10.1007/s10712-011-9119-1.

Stammer, Detlef, Cazenave, Anny, Ponte, Rui M., Tamisiea, Mark E., 2013. Causes for contemporary regional sea level changes. Annual Review of Marine Science 5, 21–46. http://dx.doi.org/10.1146/annurev-marine-121211-172406.

Ducet, N., Le Traon, P.-Y., Reverdin, G., 2000. Global high-resolution mapping of ocean circulation from TOPEX/Poseidon and ERS-1 and -2. Journal of Geophysical Research 105, 19477–19498. http://dx.doi.org/10.1029/2000JC900063.

Fu, L.-L., Qiu, B., 2002. Low-frequency variability of the North Pacific Ocean: the roles of boundary- and wind-driven baroclinic Rossby waves. Journal of Geophysical Research 107, 3220. http://dx.doi.org/10.1029/2001JC001131.

Hsin, Y.-C., Qiu, B., 2012. Seasonal fluctuations of the surface North Equatorial Countercurrent (NECC) across the Pacific basin. Journal of Geophysical Research 117, C06001. http://dx.doi.org/10.1029/2011JC007794.

Kessler, W.S., 1990. Observation of long Rossby waves in the northern tropical Pacific. Journal of Geophysical Research 95, 5183–5217. http://dx.doi.org/10.1029/JC095iC04p05183.

Kessler, William S., 2002. Mean three-dimensional circulation in the northeast tropical Pacific*. Journal of Physical Oceanography 32, 2457–2471.

Kessler, William S., McCreary, Julian P., 1993. The annual wind-driven Rossby wave in the subthermocline equatorial Pacific. Journal of Physical Oceanography 23, 1192–1207. http://dx.doi.org/10.1175/1520-0485(1993)023<1192:TAWDRW>2.0.CO;2.

Köhl, A., Stammer, D., 2008. Decadal sea level changes in the 50-year GECCO ocean synthesis. Journal of Climate 21, 1876–1890. http://dx.doi.org/10.1175/2007JCLI2081.1.

Köhl, A., Stammer, D., Cornuelle, B., 2007. Interannual to decadal changes in the ECCO global synthesis. Journal of Physical Oceanography 37, 313–337. http://dx.doi.org/10.1175/JPO3014.1.

Large, Yeager, 2004. Diurnal to decadal global forcing for ocean and sea-ice models: the data sets and flux climatologies (TN-460 + STR, NCAR, 105 pp.).

Le Traon, P.-Y., Nadal, F., Ducet, N., 1998. An improved mapping method of multi-satellite altimeter data. Journal of Atmospheric and Oceanic Technology 25, 522–534.

Locarnini, R.A., Mishonov, A.V., Antonov, J.I., Boyer, T.P., Garcia, H.E., Baranova, O.K., Zweng, M.M., Johnson, D.R., 2010. World ocean atlas 2009, volume 1: temperature. In: Levitus, S. (Ed.), NOAA Atlas NESDIS 68. U.S. Government Printing Office, Washington, D.C. (184 pp.).

Lombard, A., Garric, G., Penduff, T., 2009. Regional patterns of observed sea level change: insights from a 1/4° global ocean/sea-ice hindcast. Ocean Dynamics 59, 433–449. http://dx.doi.org/10.1007/s10236-008-0161-6.

Lorbacher, K., Marsland, S.J., Church, J.A., Griffies, S.M., Stammer, D., 2012. Rapid barotropic sea level rise from ice sheet melting. Journal of Geophysical Research 117, C06003. http://dx.doi.org/10.1029/2011JC007733.

McBride, J., Haylock, M., Nicholls, N., 2003. Relationships between the maritime continent heat source and the El Niño-southern oscillation phenomenon. Journal of Climate 16, 2905–2914. http://dx.doi.org/10.1175/1520-0442(2003)016<2905:RBTMCH>2.0.CO;2.

McGregor, Shayne, Gupta, Alexander Sen, England, Matthew H., 2012. Constraining wind stress products with sea surface height observations and implications for Pacific Ocean sea level trend attribution*. Journal of Climate 25, 8164–8176. http://dx.doi.org/10.1175/JCLI-D-12-00105.1.

Merrifield, M.A., Maltrud, M.E., 2011. Regional sea level trends due to a Pacific trade wind intensification. Geophysical Research Letters 38, L21605. http://dx.doi.org/10.1029/2011GL049576.

Merrifield, M.A., Thompson, P.R., Lander, M., 2012. Multidecadal sea level anomalies and trends in the western tropical Pacific. Geophysical Research Letters 39, L13602. http://dx.doi.org/10.1029/2012GL052032.

Meyers, G., 1979. On the annual Rossby wave in the tropical North Pacific Ocean. Journal of Physical Oceanography 9, 663–674. http://dx.doi.org/10.1175/1520-0485(1979)009<0663:OTARWI>2.0.CO;2.

Piecuch, C.G., Ponte, R.M., 2011. Mechanisms of interannual steric sea level variability. Geophysical Research Letters 38, L15605. http://dx.doi.org/10.1029/2011GL048440.

Piecuch, C.G., Ponte, R.M., 2012. Buoyancy-driven interannual sea level changes in the southeast tropical Pacific. Geophysical Research Letters 39, L05607. http://dx.doi.org/10.1029/2012GL051130.

Ponte, R.M., 2006. Oceanic response to surface loading effects neglected in volume-conserving models. Journal of Physical Oceanography 36, 426–434. http://dx.doi.org/10.1175/JPO2843.1.

Ponte, R.M., 2012. An assessment of deep steric height variability over the global ocean. Geophysical Research Letters 39, L04601. http://dx.doi.org/10.1029/2011GL050681.

Qiu, B., 2002. Large-scale variability in the midlatitude subtropical and subpolar North Pacific Ocean: observations and causes. Journal of Physical Oceanography 32, 353–375. http://dx.doi.org/10.1175/1520-0485(2002)032<0353:LSVITM>2.0.CO;2.

Qiu, B., Chen, S., 2006. Decadal variability in the large-scale sea surface height field of the south Pacific Ocean: observations and causes. Journal of Physical Oceanography 36, 1751–1762. http://dx.doi.org/10.1175/JPO2943.1.

Qiu, B., Chen, S., 2010. Interannual-to-decadal variability in the bifurcation of the North Equatorial Current off the Philippines. Journal of Physical Oceanography 40, 2525–2538. http://dx.doi.org/10.1175/2010JPO4462.1.

Qiu, B., Chen, S., 2012. Multidecadal sea level and gyre circulation variability in the northwestern tropical Pacific Ocean. Journal of Physical Oceanography 42, 193–206. http://dx.doi.org/10.1175/JPO-D-11-061.1.

Qiu, B., Joyce, T.M., 1992. Interannual variability in the mid and low-latitude western North Pacific. Journal of Physical Oceanography 22, 1062–1079. http://dx.doi.org/10.1175/1520-0485(1992) 022<1062:IVITMA>2.0.CO;2.

Timmermann, A., McGregor, S., Jin, F.-F., 2010. Wind effects on the past and future regional sea level trends in the southern Indo-Pacific. Journal of Climate 23, 4429–4437. http://dx.doi.org/10.1175/2010JCLI3519.1.

Tozuka, T., Kagimoto, T., Masumoto, Y., Yamagata, T., 2001. Simulated multiscale variations in the western tropical Pacific: the Mindanao Dome revisited. Journal of Physical Oceanography 32, 1338–1359. http://dx.doi.org/10.1175/1520-0485(2002)032<1338:SMVITW>2.0.CO;2.

Vega, A., du-Penhoat, Y., Dewitte, B., Pizarro, O., 2003. Equatorial forcing of inter-annual Rossby waves in the eastern South Pacific. Geophysical Research Letters 30, 1197. http://dx.doi.org/10.1029/2002GL015886.

Vinogradov, S.V., Ponte, R.M., Heimbach, P., Wunsch, C., 2008. The mean seasonal cycle in sea level estimated from a data-constrained general circulation model. Journal of Geophysical Research 113, C03032. http://dx.doi.org/10.1029/2007JC004496.

Vivier, F., Kelly, K.A., Thompson, L., 1999. The contributions of wind forcing, waves, and surface heating to sea surface height observations in the Pacific Ocean. Journal of Geophysical Research 104, 20767–20788. http://dx.doi.org/10.1029/1999JC900096.

Wang, C., 2000. On the atmospheric responses to tropical Pacific heating during the mature phase of El Niño. Journal of the Atmospheric Sciences 57, 3767–3781.

Wang, Bin, Wu, Renguang, Lukas, Roger, 2000. Annual adjustment of the thermocline in the tropical Pacific Ocean. Journal of Climate 13, 596–616.

Weisberg, R.H., Wang, C., 1997. Slow variability in the equatorial west-central Pacific in relation to ENSO. Journal of Climate 10, 1998–2017.

Wyrtki, K., 1975. El Niño—the dynamic response of the equatorial Pacific Ocean to atmospheric forcing. Journal of Physical Oceanography 5, 572–584.

Yu, L., Jin, X., Weller, R.A., 2008. Multidecade Global Flux Datasets from the Objectively Analyzed Air–Sea Fluxes (OAFlux) Project: Latent and Sensible Heat Fluxes, Ocean Evaporation, and Related Surface Meteorological Variables. OA-2008-1 Woods Hole Oceanographic Institution (64 pp.).

Zebiak, S.E., 1990. Diagnostic studies of Pacific surface winds. Journal of Climate 3, 1016–1031.